*Pure Appl. Chem.*, Vol. 85, No. 7, pp. 1487–1498, 2013.
http://dx.doi.org/10.1351/PAC-CON-13-04-01


# Photogeneration and reactions of benzhydryl cations and radicals: A complex sequence of mechanisms from femtoseconds to microseconds*

Christian F. Sailer and Eberhard Riedle‡

*Lehrstuhl für BioMolekulare Optik, Ludwig-Maximilians-Universität (LMU), München, Germany*

*Abstract*: Benzhydryl radicals and cations are reactive intermediates central to the understanding of organic reactivity. They can be generated from benzhydryl halides by UV irradiation. We performed transient absorption (TA) measurements over the range from femtoseconds to microseconds to unravel the complete reaction scheme. The 290–720-nm probe range allows the unambiguous monitoring of all fragments. The appearance of the radical is delayed to the optical excitation, the onset of the cation signal is found even later. Ab initio calculations show that this non-rate behavior in the 100 fs range is due to wavepacket motion from the Franck–Condon region to two distinct conical intersections. The rise of the optical signal with a quasi-exponential time of 300 fs is assigned to the planarization and solvation of the photoproducts. The bond cleavage predominantly generates radical pairs. A subsequent electron transfer (ET) transforms radical pairs into ion pairs. Due to the broad interradical distance distribution and the distance dependence, the ET is strongly non-exponential. Part of the ion pairs recombine geminately. The ET and the recombination are terminated by the depletion of close pairs and diffusional separation. The remaining free radicals and cations undergo further reactions in the nanosecond to microsecond regime.

*Keywords*: conical intersections; electron transfer; femtosecond photodissociation; geminate recombination; radical and ion pairs; Smoluchowski-type diffusional separation.

## INTRODUCTION

Carbocations are key intermediates in many organic reactions [1]. They can be generated by photoinduced heterolysis of organic halides such as R-Cl or other precursors [2]. The photolysis of these precursors can also lead to the generation of carbon-centered radicals. Both species are highly reactive and found on the nanosecond timescale after UV excitation of the precursor benzhydryl chloride ($Ph_2CHCl$) [3,4]. The benzhydryl cations can be utilized for a deep microscopic understanding of $S_N1$ reactions in solution [5]. At first sight, the early reaction steps leading to the chemically relevant fragment populations might not seem very important, as the large majority of bimolecular reactions proceed at best in the diffusional limit. Yet, the early events have been investigated in great detail by Peters and co-workers [6–10]. Their aim was not only the elucidation of the bond cleavage and the subsequent reaction

**Pure Appl. Chem.* **85**, 1257–1513 (2013). A collection of invited papers based on presentations at the XXIV$^{th}$ IUPAC Symposium on Photochemistry, Coimbra, Portugal, 15–20 July 2012.
‡Corresponding author

steps, but the hope to obtain information on the rates and barriers for the reverse processes leading to bond formation [10].

We have performed transient absorption (TA) measurements on $Ph_2CHCl$ and derivatives with the necessary temporal resolution to fully unravel the bond cleavage process and the subsequent stabilization to the final benzhydryl radical and cation. Broadband transient spectroscopy allows us a complete overview of the evolving spectral signatures. The spectra of the precursor and the products are well separated, and the dynamics can be recorded with 40 fs time resolution in two-color and broadband measurements in a thin cuvette or a free-flowing liquid jet [11].

The various aspects of these investigations have been described in a number of detailed reports [12–17]. In this article we want to give an overview of the full range of processes occurring from the earliest femtosecond times out to microseconds. As illustration, examples differing from the originally described ones are used. This shows, in addition to the full course of reaction steps, that the main features are qualitatively independent of the particular system studied. The quantitative details do, however, vary as would be expected from the wealth of results gained from preparative chemistry and the investigation of carbocation reactivity [5].

## TRANSIENT ABSORPTION SPECTROSCOPY ON MULTIPLE TIMESCALES

To monitor the ultrafast kinetics of benzhydryl halides after UV excitation, we use a femtosecond broadband pump–probe set-up that has been described in detail [18]. Briefly, a Ti:sapphire amplifier system (CPA 2001, Clark-MXR) with a repetition rate of 1 kHz is used to pump a noncollinear optical parametric amplifier (NOPA) which provides pulses with a center wavelength of 540 nm [19]. After compression and frequency doubling in a BBO crystal (100 µm thickness) we achieve pump pulses with a center wavelength of around 270 nm and 30 fs duration. The beam with a pulse energy of ~200 nJ is focused with a spot size of 100–150 µm (FWHM) into a 120-µm flow cell containing the sample solution with an optical density of about 0.3 at the excitation wavelength. A supercontinuum (290–720 nm) is generated and used as probe by focusing another part of the Ti:sapphire laser into a rotating $CaF_2$ (4 mm thickness) disk. The relative polarization of pump and probe pulses is set to the magic angle (54.7º) to avoid contributions from the rotational relaxation to the observed kinetics. A computer-controlled delay line is used to set pump–probe delays up to 2 ns. After the interaction in the sample, the probe light is dispersed with a fused silica prism and detected with a 524 pixel charge-coupled device (CCD). The chirp of the white light is corrected for prior to data analysis. The resulting temporal resolution obtained in the femtosecond spectrometer ranges from 50 fs for probe wavelengths close to the pump wavelength up to 100 fs for distant ones. This deterioration of the temporal resolution is due to the group velocity mismatch in the sample cell [20].

For TA measurements on the ns timescale we use a pulsed nanosecond laser system (NT242, Ekspla) with 1 kHz repetition rate and integrated OPO for spectral tunability to pump the sample. The nanosecond laser is externally triggered and electronically synchronized with the Ti:sapphire amplifier system, running at 1 kHz repetition rate as well. We still use the supercontinuum as described above for spectrally resolved probing. Using the same probe pulses and polychromator affords a high degree of precision in comparing the evolution of spectral features over the large range of delay times. The pump–probe delay $\Delta t$ is set by a computer-controlled delay generator, which introduces a specified temporal delay $\Delta t$ in the electronic trigger pulse from the master oscillator before the pulse triggers the release of the nanosecond excitation pulse. This set-up for TA spectroscopy, combining two electronically connected laser sources, provides a temporal resolution better than 2.5 ns and allows recording TA spectra up to temporal delays of some 100 µs.

To obtain kinetics from the TA data, we apply a multiexponential fit function augmented with a stretched exponential

$$\Delta\mathrm{OD}(t) = \mathrm{IRF}(t) \otimes \left\{ \Theta(t) \cdot \left[ \sum_i A_i \exp\left(-t/\tau_i\right) + A_{\mathrm{SE}} \exp\left[-\left(t/\tau_{\mathrm{SE}}\right)^{\beta}\right] + \mathrm{const.} \right] \right\} \quad (1)$$

The Heaviside function models the appearance of the signal at the time of the pump pulse, and the convolution with the instrument response function IRF($t$) describes the finite temporal resolution. The stretched exponential is not typically used for fitting kinetic data in related contexts. As described below, it is, however, well suited to model diffusive processes. The constant term models any long-living products like free radicals or cations. For the present work, it suffices to use the fitting function for individual wavelengths or small ranges as the different reaction intermediates display well-separated spectral signatures. A global fit analysis does not have to be performed. We do, however, observe systematic shifts of the bands that can be directly related to the underlying kinetics [13]. To precisely detect these shifts, a multistage determination of the band maximum position is performed [16].

The technical accuracy of the time constants reported throughout this report is typically better than 5 %. The systematic uncertainty due to the particular fit model chosen might by considerably larger. When the same model is used to compare two different situations, e.g., differing leaving groups, solvents, or substituents, the relative changes are not subjected to this uncertainty.

## TEMPORAL EVOLUTION OF THE REACTION INTERMEDIATES

The first electronic absorption of benzhydryl halides is found around 270 nm. It corresponds to the $S_1 \leftarrow S_0$ transition located on the benzene rings. This renders the transition rather weak with a molar absorption coefficient around $10^3$ l/mol·cm. After UV excitation, both homolysis and heterolysis (see Fig. 1c) occur on the sub-picosecond timescale. The resulting benzhydryl radicals and cations have very strong absorptions on the order of $5 \cdot 10^4$ l/mol·cm [3]. Figure 1b shows the TA changes over the time range from tens of femtoseconds out to a delay of 2 ns for tol(Ph)CHCl in $CH_3CN$ (for the molecular structure, see Fig. 1c). In Fig. 1a, the transient spectrum at 20 ps is shown. Clearly, the radical absorption at 330 nm and the cationic one at 450 nm are seen and can be easily separated. Both signatures also

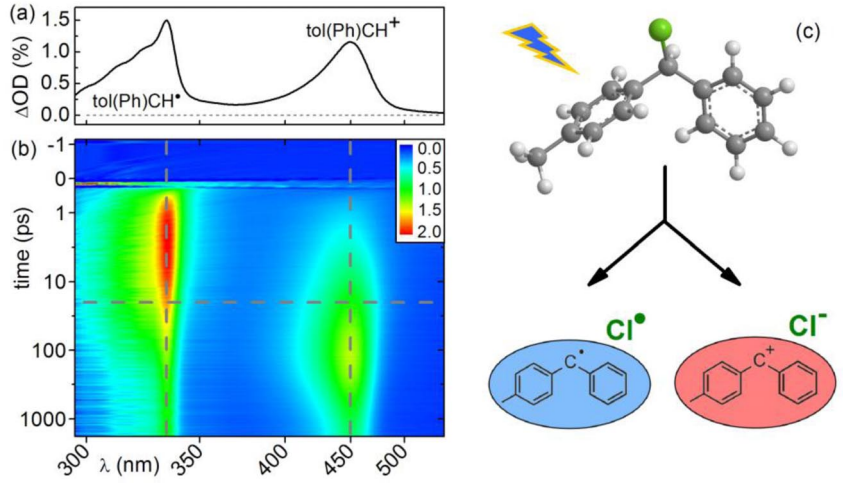


**Fig. 1** (a) Transient spectrum at a pump–probe delay of 40 ps and (b) false color representation of the 2D TA data matrix of tol(Ph)CHCl in $CH_3CN$ after 270 nm UV excitation. The delay time axis is linear between –1 and 1 ps and logarithmic beyond 1 ps. (c) Scheme of the ultrafast bond cleavage.

do not overlap with any absorption features of the precursor tol(Ph)CHCl. As with all related derivatives of the diphenylmethyl halides substituted at the phenyl rings, a complex temporal evolution of the optical signatures is found. The optical signatures can be directly related to the concentration of the radicals and cations for times beyond a few hundred femtoseconds. The transient spectroscopy, therefore, readily monitors the ultrafast chemical processes.

The most pronounced observation that can be directly deduced from the transient spectra is the fact that the radical concentration increases extremely fast after the pump pulse. It does, however, decrease again in the tens of picoseconds range. The cation concentration, on the other hand, increases more slowly and decreases in the range of hundreds of picoseconds. A closer inspection shows that both the radical decrease and the cation increase can be best modeled with a stretched exponential (see eq. 1) with a time constant $\tau_{SE}$ of 18.7 ps, corresponding to an average time of 37.4 ps for the value of $\beta = 0.5$. A stretched exponential is indicative of a diffusive process, in contrast to a purely kinetic process that is well modeled by the basic exponential decay. The overall behavior of tol(Ph)CHCl is similar to the parent $Ph_2CHCl$, but somewhat slower than the $\tau_{SE}$ = 11.1 ps observed there. This immediately signals that the substitution changes the details of the chemical dynamics.

The synchronous decrease of radical concentration and increase of cation concentration is due to an electron transfer (ET) within radical pairs. As will be discussed below, we have to conclude that the radicals (as well as the ions generated by direct heterolysis) are not all produced in close contact, but with a wide distribution of distances between the benzhydryl fragment and the chlorine. Depending on the details of the distribution and the driving force for the ET as well as the polarity of the solvent, varying overall yields for the ET are found. For $Ph_2CHCl$ we find $Y_{ET}$ = 43 % that increases to 73 % for tol(Ph)CHCl. The substitution increases the conversion to cations while the primary bond cleavage yield is very similar. The decrease in the cation concentration is found to proceed with times of 138 and 166 ps. Microscopically, it can be understood as geminate recombination that is only possible as long as the ions have not separated too much. The slow-down of the processes in tol(Ph)CHCl finally results in an increase of the long-lasting concentration of free cations from 6 % for $Ph_2CHCl$ to 11 %. So with equal numbers of photons absorbed, roughly twice as many tol(Ph)$CH^+$ ions result as $Ph_2CH^+$. These are the cations that can be used for kinetic experiments determining the reactivity [21–23].

## HOMOLYSIS AND HETEROLYSIS VIA TWO CONICAL INTERSECTIONS

Figure 2 shows high temporal resolution traces of the radical (blue, 330 nm) and cation (red, 430 nm) absorption signal around zero pump–probe delay and up to 2.5 ps for $Ph_2CHBr$ in $CH_3CN$ after 270 nm UV excitation. The spectral signatures of the bromide precursor and the fragments are very similar to the ones found for $Ph_2CHCl$. For both bond cleavage channels, the signal rises within the cross-correlation of the experiment, levels off, and then increases further with some delay. The second increase is not anymore limited by the temporal resolution of the experiment but proceeds with an effectively exponential behavior of about 300 fs. Such a 300 fs increase of the signal has been found for practically all precursor molecules studied and in various solvents [13].

The first increase in the fragment signals can be assigned to excited-state absorption of the precursor. This is concluded from the very broad and unstructured spectral distribution of this ultrafast signal component. In similar measurements on $Ph_2CHCl$ we find the same signatures at the very earliest times and even a slight decrease for the next tens of femtoseconds. In this time range, the originally generated excited-state wavepacket evolves away from the Franck–Condon region. Depending on the interplay between the $S_1$ potential energy surface and the higher ones, a slight change of signal will result.

Most importantly, we find the subsequent increase of the radical signal at 330 nm to be delayed by about 105 fs with respect to the optical excitation. Similarly, the onset of the cation signal at 430 nm shows up at a delay of 210 fs. For $Ph_2CHCl$ we find delay times of 80 and 125 fs [17]. From recent ab initio calculations we can conclude that this non-rate behavior is indeed due to the wavepacket motion in the Franck–Condon region and its subsequent evolution along the dissociation coordinate through

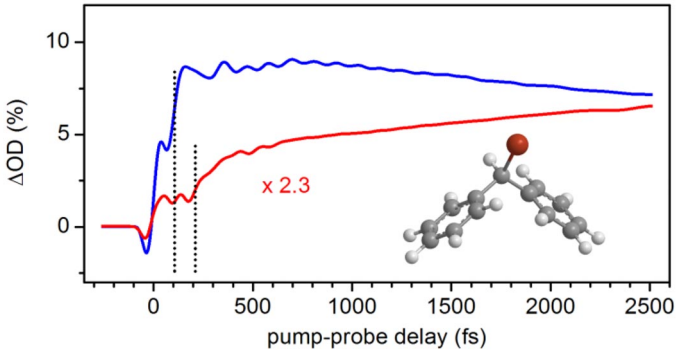


**Fig. 2** TA at the maximum of the radical peak (blue line) and the cation peak (red line, scaled for better visibility) after 270 nm excitation of $Ph_2CHBr$ in $CH_3CN$. The dotted vertical lines are shown as help to recognize the delayed impulsive increase in signal.

conical intersections [24]. Cation and radical generation occur via two distinct conical intersections, leading to different onset times for the product signals. A non-rate behavior is expected for an ultrafast process occurring through conical intersections as the nuclear degrees of freedom are far from equilibrated [25].

The further increase of the optical signal at the spectral position of the equilibrated fragment with a quasi-exponential rise time of about 300 fs has already been analyzed in detail [13]. First-principles molecular dynamics simulations show that this rise can be assigned to the planarization of the photoproducts and the solvent reorganization after the bond cleavage, the accompanying evolution of electronic states, and the associated increase in oscillator strength. Therefore, the dynamics cannot properly be described by a statistical rate, but rather the relaxation of the fragments and the solvent shell has to be taken into account.

This solvation and planarization is illustrated in Fig. 3. Originally, the precursor with its ground-state charge distribution is equilibrated with the polar solvent (preferentially $CH_3CN$ in our investigations). The optical excitation changes the intramolecular charge distribution and also starts the geo-

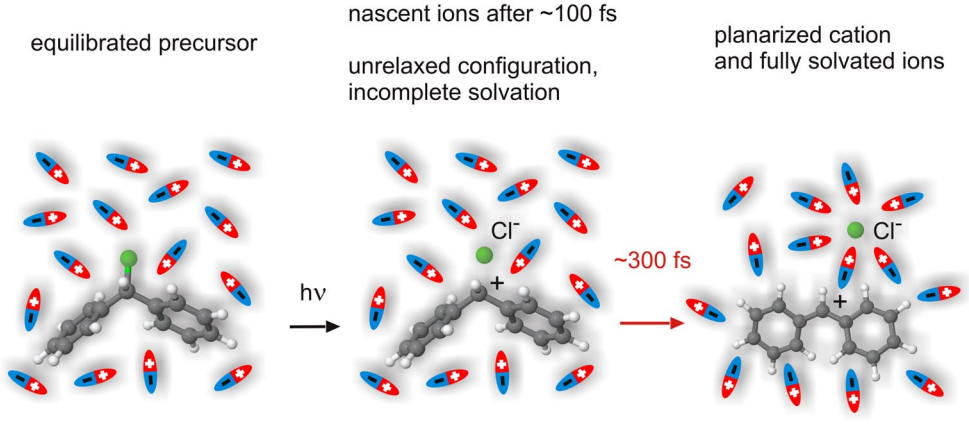


**Fig. 3** Temporal change of the configuration of the solute and the surrounding solvent molecules. Before the excitation, the precursor and the solvent molecules are in a favorable configuration. The photo-induced bond cleavage is extremely fast and does not allow for a simultaneous rearrangement of the generated ionic fragments and the solvent shell. Only within the next hundreds of femtoseconds, the cation planarizes and the ions are fully solvated by the surrounding solvent.

metric evolution. The solvent starts to react by rearranging, but this is limited by the finite response time [26]. At around 100 fs, the bond cleavage occurs and a further change in molecular charge distribution results that the solvent has to respond to. The fragments (benzhydryl radicals as well as cations) have a quasi-planar equilibrium geometry due to the $sp^2$ hybridization of the central carbon. As the original geometry was given by the $sp^3$ hybridization, a planarization has to occur. The observed signal increase is a consequence of the interplay of these processes. The processes cause a simultaneous change of the absorption signatures of benzhydryl cations and radicals. A strong increase of the oscillatory strength and a significant peak shift of the band are observed [13].

Since the bond cleavage and the solvation occur on a similar timescale, it is likely that the potential energy surfaces are influenced dynamically during the evolution of the wavepacket. As the calculations available so far were performed mainly in the gas phase, further theoretical efforts are needed to gain a deeper understanding of the solvent influence. A possible experimental approach to directly investigate the role of the solvent on the bond cleavage process was recently described by Kubarych and co-workers [27] within the framework of vibrational Stark-effect spectroscopy. Since it allows one to observe the ultrafast response of the solvent shell to changes in the charge distribution of the solute, it could allow one to track the course of the bond cleavage process.

In the recordings shown in Fig. 2, clearly oscillatory signal contributions are seen on top of the quasi-exponential signal rise. The frequency is about 300 $cm^{-1}$ for the radical and 350 $cm^{-1}$ for the cation. Both frequencies are also found in the slight variation of the peak positions [12,16]. We can assign the oscillations to a symmetric stretch motion of the phenyl rings relative to the central carbon [15]. The observation of wavepacket signatures is not unusual for ultrafast excitation conditions. However, in the photolysis of $Ph_2CH$-Br the wavepacket motion is in the photochemical products. The bond cleavage proceeds so fast that an impulsive excitation of the vibrational motion occurs. The stabilization of the radical and the cation leads to an increased electron density in the vicinity of the central carbon. Such an increase in electron density leads in turn to an impulsive shortening of the bonds and the suggested vibrational motion.

## CONVERSION OF RADICAL PAIRS TO ION PAIRS BY ELECTRON TRANSFER

The bond cleavage predominantly generates radical pairs. Since the ion pair is energetically more favorable in polar solvents like acetonitrile, a subsequent ET reaction can transform the radical pair into an ion pair [16,28]. The observed ET dynamics are strongly non-exponential, they can be perfectly fitted by a stretched exponential with $\beta = 0.5$. The resulting fit is shown in Fig. 4 together with the measured TA.

The decrease in radical population and the increase in cation population proceeds rapidly at first. From this observation we have to conclude that the ET coupling strength is quite high. On the other hand, nearly half of the radicals eventually survive. These two seemingly contradicting observations can be reconciled by the assumption of a broad inter-radical distance distribution generated by the homolysis, originating from the high kinetic energy of the fragments acquired during the bond cleavage. This means that by far not all the radical pairs are in contact. A similar broad distribution was reported for photo-detached electrons from $I^-$ [29]. The underlying assumption of all previous interpretations on the reaction dynamics of photo-excited benzhydryl halides was that homolysis would exclusively lead to geminate radical pairs (GRPs) [6–10]. We see no good arguments for this assumption. Instead, the broad inter-radical distance distribution and the distance dependence of the ET readily lead to the observed deviation from exponential kinetics. The close pairs of radicals nearly completely undergo ET while the more distant ones can escape ET and eventually separate to free radicals.

It is interesting to note that the ET-based conversion from radical pairs to ion pairs falls off with a stretched exponential of $\tau_{SE} = 2.1$ ps (corresponding to an average life time of 4.2 ps) for $Ph_2CHBr$ in $CH_3CN$. In an earlier investigation with 20 ps resolution this important early contribution was overlooked and a reaction model was developed [7,8] that the new data cannot support. This shows the

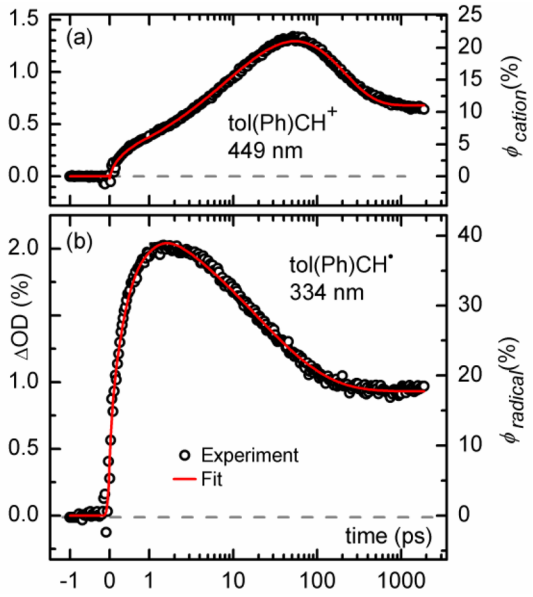


**Fig. 4** Temporal evolution of the signal (black circles) of (a) the benzhydryl cation and (b) the benzhydryl radical in $CH_3CN$. The cation and radical quantum yields $\Phi_{cation}$ and $\Phi_{radical}$ are indicated on the right. Fits are shown in red. For details, see text.

importance to use sufficient temporal resolution and a broad detection range to actually catch all intermediate species and reaction steps.

## DIFFUSIONAL SEPARATION AND GEMINATE RECOMBINATION

The ET from the benzhydryl radical to the chlorine radical leads to the major part of the benzhydryl cation population observable in polar solvents on the pico- to nanosecond timescale. It is terminated as soon as the average separation between the radicals making up a pair is too large. A large part of the temporarily generated cations, however, cannot be observed on timescales longer than 1 ns since they undergo an efficient geminate recombination with the anionic leaving group. Again, this reaction is terminated if the distance between the ions becomes too large. The net result of this sequence of processes is the increase of the cation signal to a maximum at about 55 ps and a subsequent decrease to about half of the maximum value for long times. Interestingly, in less polar solvents the cation signal nearly vanishes within the first few nanoseconds [16]. This is due to the fact that the cations are less stabilized, the attraction between the cation and the chlorine anion is less shielded, and the diffusional separation becomes more difficult [30]. As a consequence, nearly all ion pairs recombine. Cations in low-polarity solvents are only available for chemical reactions over a range of a few hundred ps.

It turned out that a proper description of the found dynamics and yields can only be achieved by a microscopic description of distance distributions of radical and ion pairs which are subject to distance-dependent ET and recombination rates. The possibility of processes occurring from a wide range of configurations means a turning away from the classical modeling of such processes. A unified description of the population dynamics emerges, with smooth transitions between the distinct species considered in traditional descriptions [10,31].

The results were analyzed by a combined model of distance-dependent Marcus-type ET and Smoluchowski-type diffusion, incorporating solvent structure and hydrodynamic effects in a mean field theory of through-solvent ET [16]. A similar approach has already been employed by Fayer and co-

workers [32] for describing ET processes in dyes and by Grampp and co-workers [33] for bimolecular fluorescence quenching. As a result, all experimental observables can be reproduced with high precision simultaneously. The majority of the necessary parameters is taken from literature or determined according to well-documented scaling relations. Some parameters emerge from the analysis itself, most importantly the broad distribution of distances for the radical and ion pairs resulting from the sub-picoseconds bond cleavage. That the fragment pairs do not just occur at contact distance is in nice agreement with the conclusions drawn for the ejection distribution of solvated electrons generated by the one-photon photodetachment of aqueous $I^-$ [29].

## PEAK SHIFTS AS A PROBE FOR THE MICROSCOPIC ENVIRONMENT

The product TA peak shift determination with better than 0.1 nm precision opens up a new direct experimental observable giving access to the microscopic realm of photochemical reactions. It allows one to track the evolution of the distance distribution of the radical and ion pairs which otherwise—if at all—would only be detectable by dedicated experiments, e.g., ultrafast chemical exchange spectroscopy [34]. The application of the peak shift evaluation comprises a wide field, ranging from the observation of ultrafast intermolecular rearrangements to solvation and vibrational cooling.

The measured peak shifts for tol(Ph)CHCl in $CH_3CN$ are shown in Fig. 5a for the cation and in b for the radical. The initial large blue shift in both fragments matches the few hundred femtoseconds increase in the absorption signal and can therefore be assigned to the planarization and solvation. A subsequent weak component with 2.1 ps time for the radical is likely the further geometric relaxation. The subsequent pronounced 23 ps blue shift matches the time it takes the ET to cease. Since the observed termination of the ET is a combination of the ET itself and the diffusional separation, we assign the 23 ps as the timescale on which the radical pair distribution changes from an contact dominated regime

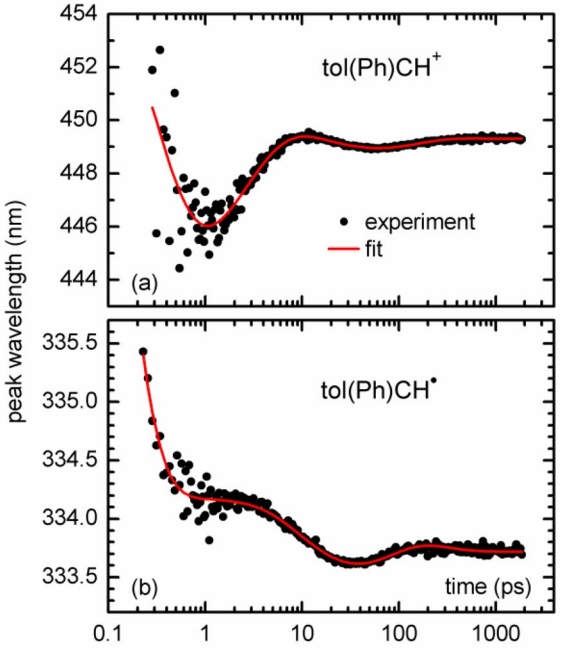


**Fig. 5** Measured (dots) and fitted (red lines) temporal evolution of the benzhydryl (a) cation and (b) radical peak position after photolysis of tol(Ph)CHCl in $CH_3CN$. For explanation of the various time regimes, see text.

to a solvent-separated one. The further weak 61 ps shift would then correspond to the full separation to free radicals.

For the cation, there is a pronounced red shift with a 3 ps time constant. The magnitude of the shift matches roughly the findings of Schneider et al. [35] who observed that the absorption maximum of free (unpaired) benzhydryl cations is red-shifted by approximately 2 nm relative to cations paired with $BCl_4^-$ anions. We would therefore like to assign this dominant component to a motion of the distance distribution to less strongly bound ion pairs. The weaker 24 and 110 ps components would then correspond to the eventual evolution to mainly free cations. For a more quantitative description, the fragment spectrum for each contributing geometry would have to be calculated and weighted by the momentary distribution [20]. The varying blue and red shift of the peak positions indicates that compensating influences have to be accounted for.

## THE FATE OF THE PHOTOFRAGMENTS

Even in solvents of rather low nucleophilicity (e.g., dichloromethane), the dynamics of the generated free benzhydryl radicals and free cations is not finished after the diffusional separation from the leaving group. Since both the radicals and cations are highly reactive, they can react on the nano- to microsecond timescale in numerous ways. The possibilities include reactions with a chlorine radical/chloride anion after diffusional (re-)encounter, reactions with the solvent, reactions with other precursor molecules, reactions with traces of water present in the sample, or dimerization between two benzhydryl radicals which encounter by diffusion [3].

The photo-induced dynamics of $Ph_2CHCl$ in acetonitrile on the nano- to microsecond scale is shown in Fig. 6. Both benzhydryl radical and cation are present at the same spectral position as in the femto- to nanosecond measurement. They decay completely within the first microseconds, and no residual signal is found throughout the spectrum at the end of the measurement. The absorption signal evolution of both photofragments has to be fitted with the sum of two exponential functions. A small part (12 %) of the benzhydryl radical population decays with a time constant of 13 ns. Most likely these are still geminate pairs that have not separated far enough or statistically re-encounter. The major part decays with a longer time constant of 330 ns. These are believed to be the radicals that have distributed equally in the solution and slowly find a reaction partner by diffusion. Similarly, a smaller fraction (26 %) of the benzhydryl cations decays with a fast time constant of 15 ns, while the larger part decays

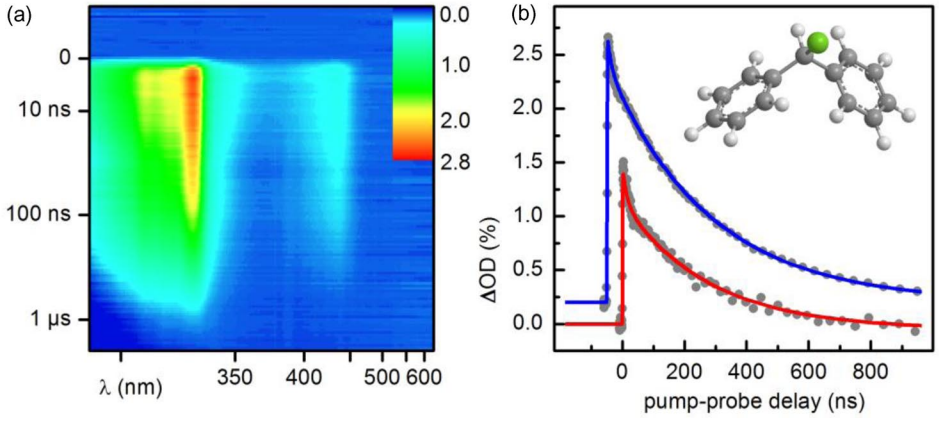


**Fig. 6** (a) Transient spectra of $Ph_2CHCl$ in $CH_3CN$ at a pump–probe delay up to 2 µs. (b) Radicals and cations undergo either non-geminate diffusional recombination with the leaving group or further reactions with the solvent or impurities.

significantly slower with a time constant of 280 ns. To determine which products are actually formed, illumination experiments are presently performed that aim to convert a sizable fraction of the benzhydryl halides into final products. The products will then be analyzed with standard chemical methods.

## SUMMARY AND CONCLUSIONS

We have performed a comprehensive set of investigations on the photogeneration of highly reactive carbocations and carbon radicals and the subsequent reactive processes. The main results are summarized and discussed in this article. For the first time, a complete photo-induced $S_N1$ reaction was observed: from the photo-induced bond cleavage and relaxation of the nascent fragments to interconversion through ET and recombination back to the precursor until complete separation to free radicals and cations. The experimental results were gained by femto- to microsecond TA spectroscopy. Novel techniques and data evaluation approaches had to be developed to understand the reactions and processes on a microscopic level. In detail, the following steps are found to be important and are depicted in Fig. 7:

- Homolysis to a benzhydryl radical and a chlorine radical is the major bond cleavage pathway of benzhydryl halides. Only less than a tenth as many ions (benzhydryl cations and chlorine anions) as radicals are initially formed. Overall, about half of the optically excited molecules undergo bond cleavage.
- Radicals and direct cations are observed with distinctly different delays.
- The bond cleavage does not follow a rate-determined evolution but has to be described by a ballistic motion toward two distinct conical intersections that are reached sequentially. The passage through these conical intersections leads to the radicals and the directly generated cations.
- The observed increase of spectroscopic signals for the radicals and direct cations on the timescale of 300 fs is due to planarization and solvation.
- A very broad distribution of fragment distances results from the ultrafast bond cleavage. The center of the distribution is shifted about half a solvent molecule away from direct contact and has a width of about two solvent molecules.
- The cations are mainly produced from radical pairs by distance-dependent ET. This means that predominantly the close radical pairs undergo ET and the remaining distribution of radicals is centered at larger distances.
- This selective reaction and further diffusional separation of the radical pairs eventually stops the ET and leads to free radicals.
- The ion pairs in close vicinity can undergo geminate recombination. The ions at larger separation can diffuse apart and form free ions.
- Both the free radicals and the free ions are highly reactive and will undergo further reactions on the timescale of hundreds of nanoseconds.

The geminate ion pair recombination was found to be the main loss channel for photogenerated benzhydryl cations in the first hundreds of picoseconds. Only in the highly polar acetonitrile a significant fraction of the carbocations escapes from the anion and becomes a free ion stable at least on the nanosecond timescale. In solvents of moderate polarity, nearly all generated cations undergo recombination with the anion. This can be rationalized by the insufficient shielding of the Coulomb attraction between the oppositely charged ions, which does not allow for the separation of the pair needed for the formation of free ions. A substantial improvement of the carbocation yield is therefore obtained when uncharged photo-leaving groups are used instead. The photolysis of benzhydryl triarylphosphonium salts leads to high yields on the nanosecond scale even in solvents of lower polarity [14].

Beyond the systems presented and discussed in this article, we believe it to be highly likely that a similar initial behavior can be found in a wide range of systems which undergo ultrafast bond cleavage. The breaking of a chemical bond usually causes geometrical rearrangements of the molecular

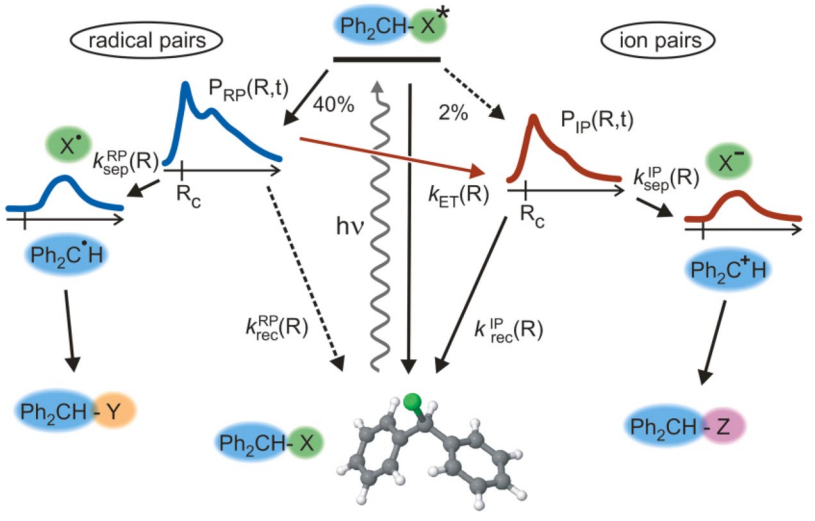


**Fig. 7** Microscopic processes involved in the bond cleavage and fragment reactions after UV excitation of benzhydryl halides $Ph_2CH$-X.

structure, and influences on the absorption signatures have to be expected. In earlier studies of the photolysis of benzhydryl chlorides with inferior time resolution, the absorption signal increase due to planarization of the nascent photofragments was interpreted as the bond cleavage. This demonstrates the high potential for the misinterpretation of rearrangement processes after the bond cleavage as the cleavage itself. In case of doubt, the assignment of optical signal changes to the bond cleavage process should therefore always be corroborated with additional experimental or theoretical evidences. Even for systems in which no bond is cleaved, a similar effect can occur. The change of absorption or emission bands after photo-excitation in the first few picoseconds is often assigned to a generic solvation process or vibrational cooling of the solute. At least for some of the systems, this could also be due to a molecular rearrangement when the ground-state configuration deviates from the one in the excited state. Once a quasi-equilibrium is reached on the ps timescale, the subsequent reaction processes can still proceed in a wide distribution of geometries. For a proper understanding and description, this distribution should be explicitly considered.

## ACKNOWLEDGMENTS

The authors thank B. P. Fingerhut, S. Thallmair, J. Ammer, H. Mayr, R. de Vivie-Riedle, and I. Pugliesi for contributions to the described research and many enlightening discussions. Financial support of this work by Deutsche Forschungsgemeinschaft through the SFB 749 and the excellence cluster "Munich Center for Advanced Photonics" (MAP) is gratefully acknowledged.

## REFERENCES

1. R. A. McClelland. In *Reactive Intermediate Chemistry*, R. A. Moss, M. S. Platz, M. J. Jones (Eds.), pp. 3–40, John Wiley, Hoboken, NJ (2004).
2. P. K. Das. *Chem. Rev.* **93**, 119 (1993).
3. J. Bartl, S. Steenken, H. Mayr, R. A. McClelland. *J. Am. Chem. Soc.* **112**, 6918 (1990).
4. H. Mayr, B. Kempf, A. R. Ofial. *Acc. Chem. Res.* **36**, 66 (2003).
5. S. Minegishi, S. Kobayashi, H. Mayr. *J. Am. Chem. Soc.* **126**, 5174 (2004).

6. K. S. Peters, B. Li. *J. Phys. Chem.* **98**, 401 (1994).
7. J. Dreyer, K. S. Peters. *J. Phys. Chem.* **100**, 15156 (1996).
8. J. Dreyer, M. Lipson, K. S. Peters. *J. Phys. Chem.* **100**, 15162 (1996).
9. M. Lipson, A. A. Deniz, K. S. Peters. *Chem. Phys. Lett.* **288**, 781 (1998).
10. K. S. Peters. *Chem. Rev.* **107**, 859 (2007).
11. A. Nemeth, J. Sperling, J. Hauer, H. F. Kauffmann, F. Milota. *Opt. Lett.* **34**, 3301 (2009).
12. C. F. Sailer, R. B. Singh, J. Ammer, E. Riedle, I. Pugliesi. *Chem. Phys. Lett.* **512**, 60 (2011).
13. B. P. Fingerhut, C. F. Sailer, J. Ammer, E. Riedle, R. de Vivie-Riedle. *J. Phys. Chem. A* **116**, 11064 (2012).
14. J. Ammer, C. F. Sailer, E. Riedle, H. Mayr. *J. Am. Chem. Soc.* **134**, 11481 (2012).
15. E. Riedle, M. Bradler, M. Wenninger, C. F. Sailer, I. Pugliesi. *Faraday Disc.* (2013). http://dx.doi.org/10.1039/C3FD00010A.
16. C. F. Sailer, B. P. Fingerhut, S. Thallmair, C. Nolte, J. Ammer, H. Mayr, R. de Vivie-Riedle, I. Pugliesi, E. Riedle. *ChemPhysChem* **14**, 1423 (2013).
17. C. F. Sailer, N. Krebs, B. P. Fingerhut, R. de Vivie-Riedle, E. Riedle. *J. Phys. Chem. Lett.* To be submitted for publication.
18. U. Megerle, I. Pugliesi, C. Schriever, C. F. Sailer, E. Riedle. *Appl. Phys. B* **96**, 215 (2009).
19. E. Riedle, M. Beutter, S. Lochbrunner, J. Piel, S. Schenkl, S. Spörlein, W. Zinth. *Appl. Phys. B* **71**, 457 (2000).
20. I. Z. Kozma, P. Krok, E. Riedle. *J. Opt. Soc. Am. B* **22**, 1479 (2005).
21. A. A. Tishkov, U. Schmidhammer, S. Roth, E. Riedle, H. Mayr. *Angew. Chem., Int. Ed.* **44**, 4623 (2005).
22. M. Baidya, S. Kobayashi, F. Brotzel, U. Schmidhammer, E. Riedle, H. Mayr. *Angew. Chem., Int. Ed.* **46**, 6176 (2007).
23. H. F. Schaller, U. Schmidhammer, E. Riedle, H. Mayr. *Chem.—Eur. J.* **14**, 3866 (2008).
24. B. P. Fingerhut, D. Geppert, R. de Vivie-Riedle. *Chem. Phys.* **343**, 329 (2008).
25. W. Domcke, D. R. Yarkony, H. Köppel. *Conical Intersections: Electronic Structure, Dynamics and Spectroscopy*, World Scientific Publishing, Singapore (2004).
26. M. L. Horng, J. A. Gardecki, A. Papazyan, M. Maroncelli. *J. Phys. Chem.* **99**, 17311 (1995).
27. C. R. Baiz, K. J. Kubarych. *J. Am. Chem. Soc.* **132**, 12784 (2010).
28. J. W. Hilborn, E. MacKnight, J. A. Pincock, P. J. Wedge. *J. Am. Chem. Soc.* **116**, 3337 (1994).
29. J. A. Kloepfer, V. H. Vilchiz, V. A. Lenchenkov, A. C. Germaine, S. E. Bradforth. *J. Chem. Phys.* **113**, 6288 (2000).
30. C. Reichardt. *Solvents and Solvent Effects in Organic Chemistry*, Wiley-VCH, Weinheim (2003).
31. D. J. Raber, J. M. Harris, P. v. R. Schleyer. In *Ions and Ion Pairs in Solvolysis Reactions in Ions and Ion Pairs in Organic Chemistry*, M. Szwarc (Ed.), pp. 248–366, John Wiley, New York (1974).
32. A. Goun, K. Glusac, M. D. Fayer. *J. Chem. Phys.* **124**, 084504 (2006).
33. A. Rosspeintner, D. R. Kattnig, G. Angulo, S. Landgraf, G. Grampp. *Chem.—Eur. J.* **14**, 6213 (2008).
34. J. Zheng, K. Kwak, J. Asbury, X. Chen, I. R. Piletic, M. D. Fayer. *Science* **309**, 1338 (2005).
35. R. Schneider, H. Mayr, P. H. Plesch. *Ber. Bunsenges. Phys. Chem.* **91**, 1369 (1987).